Towards optimal plasma actuator arrays for friction drag reduction

Towards optimal plasma actuator arrays for friction drag reduction

Journal of Physics: Conference Series **3173** (2026) 012005 doi:10.1088/1742-6596/3173/1/012005

Towards optimal plasma actuator arrays for friction drag reduction

E. Fracchia [1], **L. Antal** [1], **G. Cafiero** [1], **D. Gatti** [2], **and J. Serpieri** [1]

[1]Department of Mechanical and Aerospace Engineering, Politecnico di Torino, Turin, Italy
[2]Institute of Fluid Mechanics, Karlsruhe Institute of Technology, Karlsruhe, Germany

E-mail: edoardo.fracchia@polito.it

Abstract. An optimization framework for the design of an array of DBD plasma actuators to be eventually used for friction drag reduction from turbulent flows is presented. To investigate the plasma induced flow and eventually their effect on the incoming flow, high fidelity simulations were performed. The actuators were modeled according to body force distributions well documented in the literature. The aim of the work is to explore how different geometrical and operational parameters of the PA array affect the induced flow. First, in the optimization iterations, laminar flow simulations are carried out in order to recreate a Stokes-like flow, which can compensate for the known drag-enhancing effect caused by the plasma-jets induced downwash. Then, the effect of the optimized configuration forcing is assessed on a turbulent channel flow at $Re_\tau = 250$. Eventually, also the effect of the incoming flow on the plasma-induced flow is evaluated.

1 Introduction

Turbulent viscous drag is estimated to account for up to half of the total drag on an airliner in cruise flight; therefore, a reduction of drag would directly reduce fuel consumption. At a laboratory scale, this can be either achieved with passive approaches, such as riblets [1–4] or with active methodologies. Among the active approaches, besides the wall blowing, inducing a non-stationary spanwise pressure gradient proved to interfere with the self-generation cycle of turbulence [5] leading to reduced friction flows. This approach can be realized by oscillating the wall (OW) along the span-wise direction. This action can disrupt the turbulence coherent structures and the related higher friction events, therefore, actively reducing the skin friction drag [6, 7]. However, such a flow control approach is cumbersome to implement on real flows, limiting this approach to laboratory efforts [8].

Arrays of plasma actuators (PAs) can be realized to mimic the crossflow generated by a OW by generating synthetic jets at the wall, oscillating along the spanwise direction [9–11]. PAs, in the dielectric barrier discharge (DBD) configuration, are characterized by high-frequency response, reduced weight and size, moderate power consumption, and lack of moving parts. Moreover, they can be easily retrofitted to surfaces with complex geometries and are not too complicated and costly to be fabricated.

Different plasma actuator geometries have been proposed for different purposes [11–13]. For the present study, aiming at friction drag control, we consider the geometry shown in Figure 1, which consists of two high-voltage electrodes exposed to the flow with a grounded encapsulated electrode positioned in between. Repetition of this basic configuration along the spanwise direction leads to the construction of an array to mimic the OW effect. The spanwise repetition shall minimize the flow regions where plasma is not generated, resulting in a more homogeneous distribution of the induced control flow across the span. To go in this direction, Hehner et al. 2019 [11] introduced a 4-electrodes PA array.

PAs are electrical devices and, as such, have a wide operating range, meaning that their geometry and actuation parameters (e.g. induced jets' strength, modulation frequency, carrier frequency, duty cycle) are mostly independent and greatly influence the resulting body force and consequently the induced velocity fields [14]. Given this wide range of possible actuation parameters and their nonlinear effects, caused by the complex interaction between the flow and the plasma, when designing PA arrays for friction drag reduction, it might prove crucial to optimize the actuation (geometrical and operational) parameter space. Doing this in lab tests can be extremely lengthy, given the efforts needed to build and operate robust PAs, an alternative approach, hereby followed, considers numerical investigations.

The focus of this work will be on investigating the flow response with respect to four forcing parameters: the oscillating or modulation frequency (f_m [Hz]), the duty cycle (DC), the spanwise distance of the electrodes (λ_z [mm]) and the integral force per streamwise unit depth (F_{int} [N/m]). The flow simulations consider a channel flow, which reduces the computational cost. In the remainder of the work, all quantities will be scaled either in the inner or outer units of the related channel flow. The superscript "+" indicates inner-scaling with friction velocity u_τ and kinematic viscosity ν. The outer quantities used for scaling are: the bulk velocity $\overline{U}_b = 4.3$ m/s, the half-channel height $\overline{h} = 0.0125$ m, the modulation frequency $\overline{f}_m = 50$ Hz and the integral force $\overline{F}_{int} = 7.15$ e^{-3} N/m, being the ones reported in Reference [11].

Previous research has examined the influence of individual parameters on the flow field and how these effects can contribute to drag reduction. While investigating the effect of the oscillation period over a turbulent boundary layer, Jukes et al. 2006 [9] observed larger levels of drag reduction at increasing modulation frequencies, downstream of the actuation zone. However, as the frequency increases, the flow reaches a point where there is no longer spanwise oscillating flow, but rather a quasi-steady wall-normal jet, referred to as upwash, similar to what would happen without any modulation [15, 16]. Related to this upwash fluid motion, downwash motions also set in to compensate the mass flux. These, in the realm of friction drag control, can result in a negative effect as they contribute to the advection of higher momentum fluid towards the wall [11].

The formation of said vertical jet clearly also depends on the distance of the exposed electrodes, λ_z, which, in turn, also influences the number of streaks that are acted on simultaneously. A beneficial effect of tighter spacing between the electrodes was also observed numerically, with a different body force model [17] and with streamwise traveling waves [18]. Moreover, the appropriate distance between the electrodes ensures that the upwash and downwash counteract, as, if they are too far apart, high momentum fluid is drawn close to the wall by vortex induction [9].

The last parameter that was considered is the integral force, that is, the total force applied by the actuator on the fluid, directly linked to the induced spanwise velocity. In an experimental setup, this parameter can be easily controlled by changing the input voltage supplied to the high-voltage PA electrodes, within the limits imposed by the PA embodiment. Note that variations of the AC signal carrier frequency would also impact this parameter.

In this study, the four mentioned PAs parameters will be studied. While the final goal of the proposed research is reducing turbulent flows friction drag, this initial effort aims at finding the optimal forcing parameters leading to the desired Stokes-like flow showing the least wall-normal motions deemed detrimental as previously mentioned. To this goal the numerical setup considered first a laminar channel flow. This choice further helps with the computational cost of the envisioned study as laminar flows require less resources to statistically converge.

The found set of optimal parameters was then evaluated on a turbulent flow. While, of course, this approach by steps might not lead to the overall optimal configuration for turbulent flows friction drag reduction, it helps us building understanding on the effect of the mentioned parameters and it does so at an acceptable computational cost.

The paper is structured as follows. In Section 2, we discuss the DNS solver, the model used to estimate the body force induced by the plasma actuators and the structure of the optimization framework. Next, we address the selection of the cost function to be optimized. In Section 4, the optimal parameters obtained are evaluated in a turbulent simulation. Finally, Section 5 summarizes the findings of the study and outlines potential directions for future work.

2 Methodology

2.1 Numerical setup

The incompressible channel flow was computed with the DNS code described in References [19] and [20]. The method is based on Fourier expansions in the homogeneous directions and fourth-order accurate, compact finite-difference discretization over a variable-spacing mesh in the wall-normal direction (y). The convective terms were discretized with a third-order Runge-Kutta scheme, while the viscous term as a second-order Crank-Nicholson scheme. The simulations were run at a fixed Reynolds number of

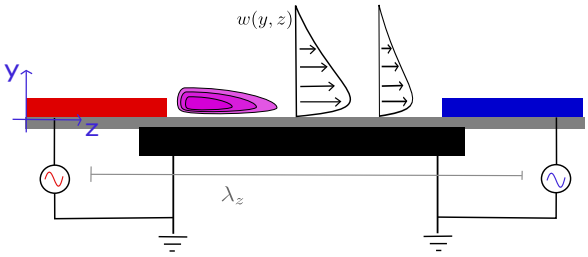

Figure 1: Schematic representation of the three electrodes PA. The two exposed high-voltage electrodes are represented with the blue and red boxes, while the black one is the grounded electrode. λ_z is the streamwise spacing between the two exposed high-voltage electrodes.

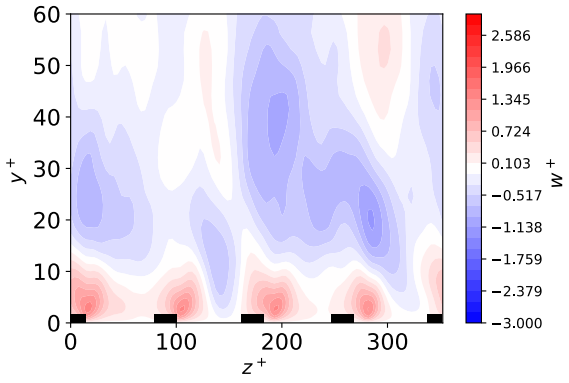

Figure 2: Inner-scaled spanwise velocity, w^+, in a cross-plane in a generic actuation phase. The black rectangles represent the PAs' exposed electrodes (height: not-to-scale).

$Re_b = U_b h/\nu = 4025$, based on the bulk velocity U_b, which corresponds to a friction Reynolds number of $Re_\tau = 250$, for the turbulent non-actuated case. Periodic boundary conditions were assumed allowing for Fourier discretization in the streamwise (x) and spanwise (z) directions. As such, in our setup, a continuous array of PAs is simulated. In other words, there is no free space along the spanwise direction among the different actuators. Therefore the PAs spanwise spacing (λ_z) coincides with the electrodes spacing, as shown in Figure 1.

A constant mass flow rate was imposed as boundary condition and only half channel was considered. An additional source term was included in the spanwise momentum equation to account for the time-varying PA-induced body force as already done in e.g. [10, 18].

For the laminar flow simulations, a spatial discretization of $n_x = 1$, $n_z = 96$ nodes and $n_y = 64$ points was chosen. In such a domain, one single actuator was considered. For the laminar flow simulations, only a single streamwise node was considered, not to let turbulence develop. The value of the laminar skin friction coefficient matches the theoretical one and the mean wall normal profile fits the Poiseuille solution. Laminar flow simulations were run for different total integration times, as the convergence time depended on the forcing period, which was not constant across the different optimization iterations. The simulation convergence was assessed by observing no significant variations in the meaningful quantities. The simulations were performed on a workstation equipped with a 12th generation Intel Core i7-12700K CPU, taking advantage of the solver's low memory requirements and parallel computing.

For the turbulent simulations, the domain was enlarged in the spanwise direction to properly accommodate turbulent structures and obtain correct flow statistics [21]. The domain size has respectively streamwise, spanwise and wall-normal lengths of $L_x^+ = 547$, $L_z^+ = 316$ and $L_y^+ = 287$. Four plasma actuators could be accommodated in this domain. The following spatial discretization was considered $n_x = 63$, $n_z = 96$ and $n_y = 83$, with grid spacings $\Delta x^+ = 9$, $\Delta z^+ = 4$, $\Delta y^+|_{y=0} = 0.2$. The turbulent simulation was run for a number of large eddies turnover times $T_{to} = 3000\ \overline{U}_b/\overline{h}$, after which no significant change in the quantities of interest was observed. The integration time step was set to $\Delta t = 1.45\, e^{-3}\, h/\overline{U}_b$ s. The Courant-Friedrichs-Lewy number of the simulations fluctuated around the value of 0.3.

An instantaneous cross-plane flow field of spanwise velocity (w^+), also showing the position of the PAs electrodes is shown in Figure 2 for illustration. The plasma-induced jets directed towards positive z are clearly visible near the wall and appear rather modulated along the spanwise direction for the chosen input forcing parameters.

2.2 Body force model

The adopted body force model is the one proposed by Suzen et al. [22]. It was chosen because it matches well experimental results and higher-fidelity simulations over a range of input signal frequencies and voltages [23]. Moreover, it is physics-based. Therefore, unlike empirical models, it computes the

body force as a function of the geometry and electrical parameters of the actuator. It is based on the assumption that the electric field is conservative and that air is weakly ionized. As a consequence, the electric potential can be decoupled in two terms: one related to the net charge density and the other to the electric field applied to the electrodes. The body force term is computed in a preprocessing step, in which the two electric potential equations are solved to compute the force components along the spanwise and wall-normal directions.

The value of the integral force, often referred to as thrust, is provided as an input to the Suzen-model solver, allowing different actuation strengths to be considered. To do so, the force distribution is rescaled so that its integral over the cross-plane matches the value specified in Reference [11]. The resulting distribution is then smoothed, interpolated onto the DNS discretization scheme, and treated as a source term in the spanwise momentum equation [10]. Plasma discharges occur only when the electric field exceeds the fluid breakdown voltage, at which point, ionization takes place. Beyond this threshold, the force exerted on the fluid has been experimentally observed to vary approximately linearly with the applied voltage. Increasing the voltage also extends the plasma region until it reaches the end of the buried electrode, causing the force distribution to vary spatially. Further increasing the supplied voltage instead does not vary much the exerted body force as most of the supplied energy is dissipated as heat.

Differences in the body force distribution were shown in the literature [10, 24] to strongly impact the effectiveness of the applied control. Nevertheless, for the sake of simplicity, we did not model the effect of the supplied voltage amplitude on the body force distribution; we just considered different values of integral force for a fixed spatial distribution. Despite this assumption, the induced control flow still undergoes modifications in both its wall-normal and spanwise extension due to the variation of the integral force. Future efforts shall consider also the effect of the PAs geometrical and operational parameters on the body force spatial distribution first, on the induced flow then and, finally, on the controlled flow.

Furthermore, we also did not consider the temporal response of the body force field to the supplied voltage modulation, given that, as previously described, we did not model the voltage signal. Therefore, we assumed the body force term to be binarily modulated between ON and OFF.

2.3 Optimization

The results of the DNS simulations are evaluated in terms of a cost function, according to which a Bayesian optimizer determines the next set of parameters. This approach was chosen due to several factors: the non-linear relationship between the cost function and the optimization parameters, the considerable computational cost of many laminar DNS evaluations, the potential presence of multiple local minima for the cost function and the lack of available information on the gradient of the cost function. The Bayesian optimizer function `bayesopt.m`, provided in the MATLAB "Statistics and Machine Learning Toolbox" [25], was employed. The chosen acquisition function for sampling was "expected improvement plus".

The overall optimization framework is represented in Figure 3: the set of optimization parameters determines the body force distribution according to the Suzen model. The Reynolds number and the channel geometry, in terms of domain nodes and points are kept fixed. After a laminar flow simulation is completed, the performance of the actuator is evaluated, over an actuation period, in terms of the chosen cost function. Two different cost functions were evaluated and which will be discussed in the next section.

3 Optimization through laminar simulations

3.1 Minimum laminar skin friction

Plasma actuators can hinder the turbulence re-generation cycle, resulting in weaker coherent structures [26]. However this actuation has also an effect on the mean flow; while the flow is accelerated in the spanwise direction, high momentum fluid is drown towards the wall, increasing the skin friction drag. As a consequence, the actuators affect the near-wall small scales, related to turbulence, but they also induce large scale streamwise vortical structures. Since the latter effect, can be unfavorable as previously mentioned, the first tested approach consisted in minimizing this term while inducing a Stokes-like flow at the wall. The effect of these streamwise vortices in terms of their related down- (up-)wash motions can be quantified in terms of the laminar skin friction coefficient, since the high (low) momentum fluid drawn towards (away from) the wall increases (decreases) the velocity gradient at the wall. The skin friction coefficient is defined as:

$$c_{f,l} = \frac{2\tau_w}{\rho U_b^2} = \frac{2\nu \left(dU/dy\right)_{y=0}}{U_b^2} \tag{1}$$

with τ_w the shear stress at the wall and ρ the fluid density.

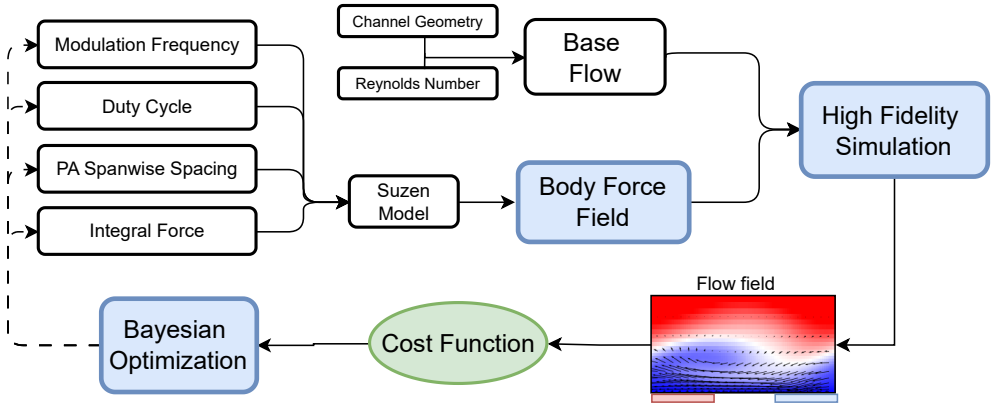

Figure 3: Optimization framework scheme: the blue boxes indicate the iteration steps where computation tasks take place, the white ones show the input variables while the green one represents the step where the cost function is evaluated.

To test this idea, simulations with different modulation frequencies were tested. The results showed that, with the current setup, the optimizer always converged to vanishing actuation configurations. A secondary minimum of $c_{f,l}$ was observed, indicating that there is in fact a range of modulation frequencies that mitigates the downwash effect. However, because the absolute minimum occurs at null forcing, the algorithm consistently retrieves that trivial solution. Simply excluding the trivial solution from the explored parameter range does not resolve the issue: the optimizer will then converge to the next available lower bound, still physically uninteresting. This highlights a limitation of using the $c_{f,l}$ cost function, it leads to minimal forcing, at least within the current optimization framework.

3.2 Oscillating wall similarity

Not only the laminar skin friction coefficient, but most metrics aiming at minimizing the downwash effect of the actuator on the mean flow would likely be affected by the issue highlighted in the previous paragraph. We therefore tested a new strategy and decided to target a velocity field that is already known to achieve drag reduction in turbulent flows. The idea was to have a cost functions that reflects the similarity between this reference field and the one induced by the actuators. In this case, the trivial solution would not achieve a lower value of the cost function. The reference velocity field must satisfy three conditions, it should: (i) achieve drag-reduction, (ii) be physically replicable with plasma actuators, and (iii) admit an explicit (analytical or empirical) expression. The last requirement is important because an analytical formulation allows to compute the reference field at the Reynolds number of choice, for the phases of the actuation period.

Based on these criteria, the velocity field generated by an oscillating wall and analytically described by Stokes' second problem was chosen as the reference case. However, it is important to recognize two key differences between the flow generated by plasma actuators and those described by the Stokes flow. First, for plasma actuators, the induced spanwise velocity does not peak at the wall but instead reaches its maximum at some distance above it, whereas, for the Stokes flow, the maximum velocity occurs directly at the wall, due to the no-slip condition. Second, the Stokes flow velocity field is homogeneous in a cross-plane along the spanwise direction, while the actuator-driven field is not, due to the discrete forcing generated by the different PAs constituting the array.

To deal with the first discrepancy, for the cost function evaluation, the computed PA-induced velocity profiles were truncated at the wall-normal position where the spanwise velocity reaches its maximum. In other words, the near-wall region ($y/\overline{h} \lesssim 0.27$), which cannot be matched by any set of PA parameters, was excluded from the optimization. The computed flow at the mid-span location between the two electrodes was compared to the Stokes flow solution to overcome the mentioned spanwise inhomogeneity of the PA-induced flow. This region is the only one where the wall-normal velocity profiles in the two half-cycles are symmetric, and thus the most similar to the OW flow [11]. Furthermore, a rapid test showed that, considering the whole velocity field in the cost function, led to significantly noisier data, thus requiring a larger number of iterations to achieve an acceptable resemblance to the reference field.

The reference OW flow field corresponds to the configuration described in Reference [27]. In that study, the maximum net power saving ($\max(P_{net})$) was obtained for an inner-scaled oscillation amplitude $W_m^+ = 4.5$ and an oscillation period of $T^+ = 125$. The net power saving is defined as the difference between the power saved and the power required for actuation, $\%P_{net} = \%P_{sav} - \%P_{act}$. The power saved is computed as the $\%P_{sav} = 100(c_{f,0} - c_f)/c_{f,0}$ and as such it is directly linked to drag reduction. The net power saved additionally takes into account the power spent for the actuation of the oscillating wall due to viscous effects. The inner scaled oscillation amplitude and period that achieved the largest net power saving in Reference [27] were chosen.. This metric was preferred over the drag reduction, since the latter is obtained with relatively large spanwise velocities, which may be difficult to achieve in practice using plasma actuators.

Having fixed these two parameters: W_m^+ and T^+, it is possible to fully determine the reference velocity field for each phase, according to the following expression:

$$w(y,t) = W_m \exp\left(-\sqrt{\frac{\omega}{2\nu}}y\right)\cos\left(\omega t - \sqrt{\frac{\omega}{2\nu}}y\right), \tag{2}$$

where $\omega = 2\pi/T$.

To identify the set of parameters that best reproduce the reference flow field, it is necessary to quantify the similarity between the simulated and reference fields. For this purpose, only the spanwise velocity component was considered as it is the only component available in the analytical expression for the OW.

Since the induced flow is periodic, this temporal variability had to be incorporated into the cost function. This was achieved by extracting wall-normal velocity profiles at different phases of the oscillation period and assembling them as columns of a matrix. The resulting representation is a matrix of size $n_y \times n_p$, where n_p is the number of phases of the modulation cycle considered and n_y the points in the wall-normal direction. It compactly represents the flow over the period and as such will be referred to as "period matrix". To assess the similarity between the reference Stokes' flow and the simulated period matrices, the cross-correlation between the two matrices was computed, where the arguments are shifted only around the second dimension, corresponding to the phases:

$$\widehat{R}_{RS}(0,d_j) = \sum_{i=1}^{n_y}\sum_{j=1}^{n_p} R(i,j)\cdot S(i+0, j+d_j), \tag{3}$$

where R refers to the reference field and S the simulated one. The cost function was then evaluated as the minimum difference between the computed cross-correlation and the reference matrix autocorrelation:

$$\Psi = \min(\widehat{R}_{RS}(0,d_j) - \widehat{R}_{RR}(0,0)). \tag{4}$$

The considered cost value Ψ tends to zero as the PAs fields approach the reference OW flow. Normalization was avoided to ensure that differences in magnitude between the two fields were preserved, otherwise two Stokes flows with different amplitude but the same oscillation period would have the same cost value.

The cross-correlation was chosen because it can account for phase shifts between the two flows to eventually rearrange the profile phases to maximize the correlation between the two period matrices. For example, if a root-mean-difference between the two matrices was used instead, the matrices phases should be first aligned. Phase alignment based on the forcing input is not difficult to obtain; however, there is no guarantee that the two flow fields are most similar when the modulation signals are aligned in time (phase), as one field results from a boundary condition, while the other is generated by a distributed body force and thus considers the flow inertia. Moreover, because the different phases are stacked as columns in the matrix, there is no constraint enforcing a fixed oscillation period. Consequently, the optimal period, scaled in inner-units, can differ from that of the reference OW flow. In the case of OW flow, the oscillation period and velocity profile shape are inherently coupled, as altering the period changes the profile. This approach allows to separately investigate the effects of these two parameters.

The phase averaged velocity profiles are shown in Figure 4. A good match between the reference OW profiles (Figure 4a) and the final optimized velocity profiles induced by the plasma actuators in quiescent flow (Figure 4b) can be observed both in terms of amplitude and temporal evolution. The effect of the interaction between the plasma-induced flow and the incoming flow is also analyzed by considering plasma actuation, with the same forcing parameters and on the same bulk flow, on a laminar (Figure 4c) and turbulent (Figure 4d) base flow. Overall, we observe the largest induced spanwise velocity for the quiescent flow case, likely caused by the absence of streamwise convection. Comparing first the profiles for the quiescent flow case (Figure 4b) with those on an incoming laminar flow (Figure 4c), we see that

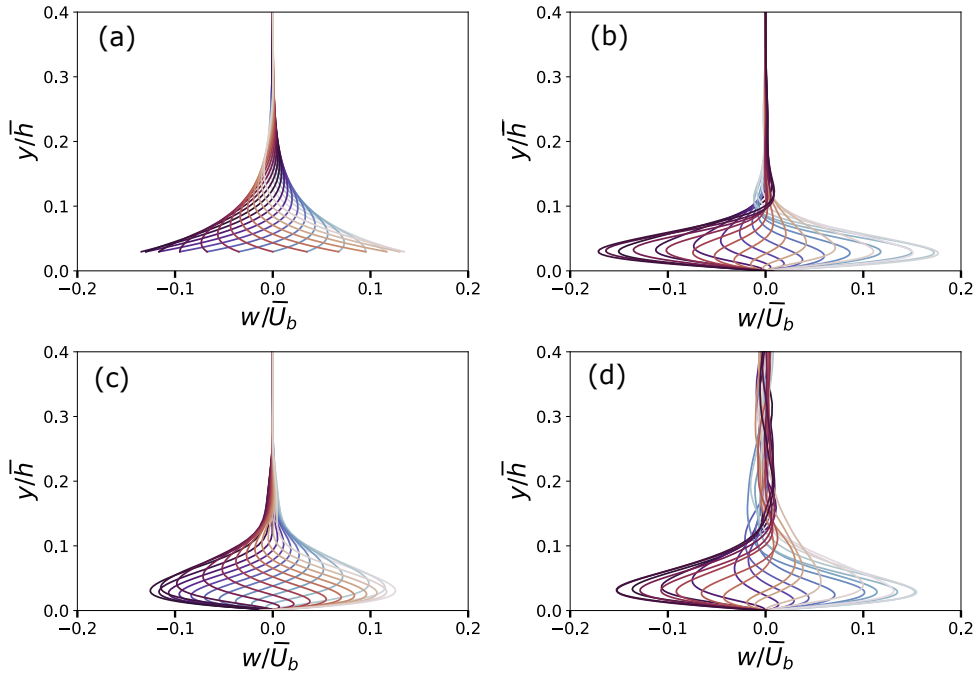

Figure 4: Outer-scaled spanwise velocity profiles, averaged along x and phases, across 24 phases: OW reference flow (a), plasma induced flow in quiescent flow (b), optimal parameters in laminar flow (c) and optimal parameters in turbulent flow (d). The OW profiles (a) are shifted to the same $\max(w/\overline{U_b})$ position of the laminar flow profiles (c), to facilitate comparison.

the secondary, opposite-sign peak of induced velocity observed for the quiescent flow case at $y/\overline{h} \approx 0.11$ is canceled for the same forcing in a laminar flow. This might be caused by the laminar flow which advects away the oppositely-directed flow generated in the other half of the modulation period, where the PAs blow in the opposite z direction. In the turbulent flow case (Figure 4d), the actuation effects appear to be confined closer to the wall compared to the laminar flow case (Figure 4c). This corresponds to the region with steeper streamwise velocity gradients. Moreover, the Reynolds stresses lead to a transport of momentum for the turbulent flow case.

It should be noted though that the differences in the induced profiles, observed in Figure 4(c and d) are not generally marked when considering outer-scaled quantities, so the laminar simulation can provide an initial indication of the mean flow behavior, whose effect can be observed in Figure 5. Nonetheless, non-linear effects between the plasma-induced flow and the incoming flow still appear to affect the applied control flow. This observation shall induce caution in following the approach hereby presented, as optimizing the control parameters on a given flow might result in different control flows on another. This might advice to directly optimize the control parameters on the final turbulent flow on which flow control will be applied. On the other side, the much cheaper laminar flow simulations allowed to explore a broad range of combinations of control parameters which would have been unfeasible with the same computational resources for turbulent flows.

Going back to the optimization results, the set of optimal parameters, scaled with the outer reference quantities, is: $f_m^* = 1.1$ ($T^{+*} = 200$), $DC^* = 0.43$, $\lambda_z^* = 1$ and $F_{int}^* = 1$. These will be referred to as optimal forcing parameters and are indicated with the * superscript. The found optimal parameters have similar values to the ones tested in Reference [11], for a quiescent flow, resulting in comparable velocity distributions.

4 Turbulent simulation with optimal parameters

To evaluate the actuation parameters obtained from optimization, a turbulent simulation was performed. With a constant mass flow rate, drag reduction implies a lower pressure gradient and thus a smaller skin friction velocity compared to the non-actuated case. Instead, the simulations show an overall drag increase in the skin friction coefficient of about 22% . Nonetheless, Figure 5 highlights regions along the

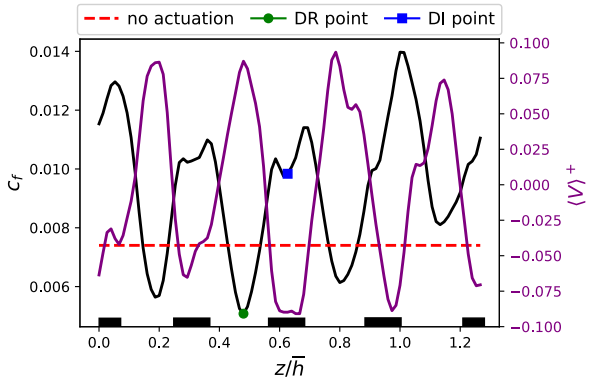

Figure 5: Time-averaged skin friction coefficient along the span, showing: the averaged non-actuated flow value (red dashed line); the maximum value of drag reduction (green dot); the center of the domain (blue square). Overlain in purple is the wall normal velocity measured at $y^+ = 10$. The black boxes indicate the PA exposed electrodes (height: not-to-scale).

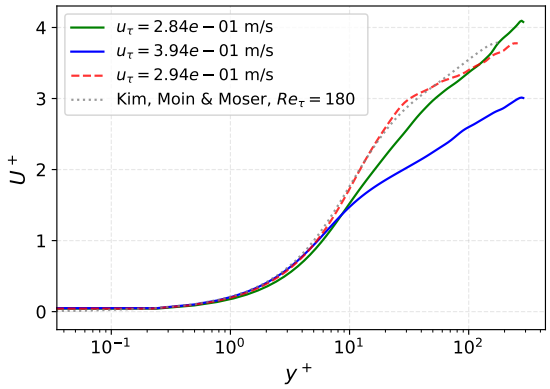

Figure 6: Wall-normal distribution of the streamwise velocity profiles for the two locations shown with the same colors on the left plot. The red dashed line is the velocity profile for the non-actuated case and the gray dotted line is a reference profile from literature [28].

spanwise direction where drag is locally reduced relative to the unforced reference case, e.g. $z/\overline{h} \approx 0.18$ and 0.44 . The maximum drag reduction is marked with a green circle, while the area above the exposed electrodes (blue rectangle) consistently coincides with increased drag. There is a clear correlation between the downwash regions, where the vertical wall-normal velocity is stronger, and the regions where the skin friction coefficient is locally increased.

To further analyze these two zones of dominant drag enhancement and reduction, Figure 6 shows local wall-normal profiles of the time-averaged streamwise velocity. Each profile is scaled with the skin friction coefficient based on the local velocity gradient at the wall and compared against the non-actuated case at a spanwise position where the skin friction coefficient matches its mean value. The non-controlled flow matches well the Reference [28]. The drag increased profiles exhibits a velocity deficit in the logarithmic layer, while the lower drag results in a profile with a decreased local skin friction velocity.

The effect of optimal PA forcing on the flow Reynolds stresses is shown in Figure 7: the streamwise variance exhibits a reduced peak, which under constant mass-flow conditions, translates into a lower pressure gradient, while the other components result magnified by the performed flow control.

Finally, we explore the actuation impact on the turbulence coherent structures in the viscous sublayer. To do so, we computed the two-point autocorrelation of streamwise velocity fluctuations at $y^+ = 10$, averaged over time ($\langle R_{uu} \rangle$) where only the stochastic fluctuations, i.e. the flow fields resulting from the difference between the instantaneous fields and the corresponding phase averaged field, were considered, as by the triple decomposition approach. Figure 8 shows the autocorrelation functions which suggest that plasma forcing may be effective in reducing the streaks streamwise coherence, as indicated by a faster decay of correlation in the streamwise direction. This suggests a positive effect in the view of deploying PA arrays for turbulent flows friction drag reduction. Nevertheless, the reported detrimental wall-normal motions need to be reduced to achieve an overall positive (drag reducing) effect.

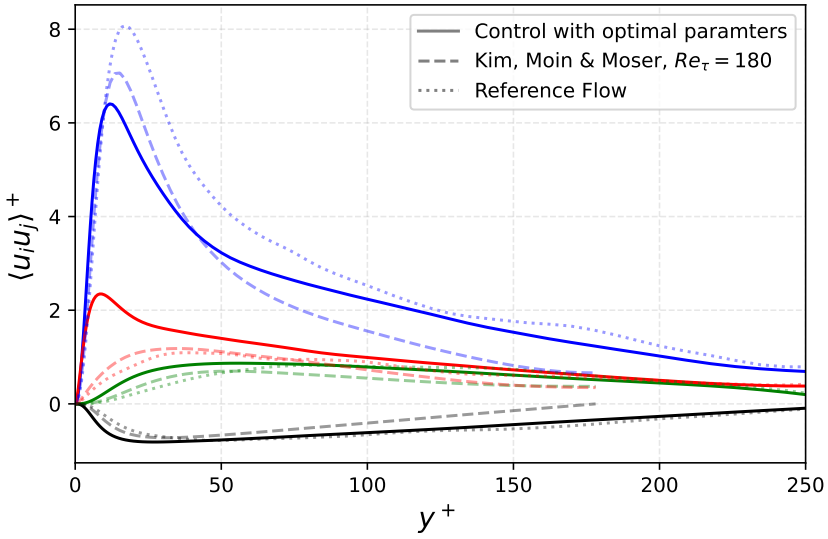

Figure 7: Reynolds stresses from the current simulation with optimized parameters (full lines), from Moin et al. [28] at $Re_\tau = 180$ (dashed lines), and in the simulated reference flow (dotted lines): $\langle uu \rangle^+$ (—), $\langle ww \rangle^+$ (—), $\langle vv \rangle^+$ (—), and $\langle uv \rangle^+$ (—).

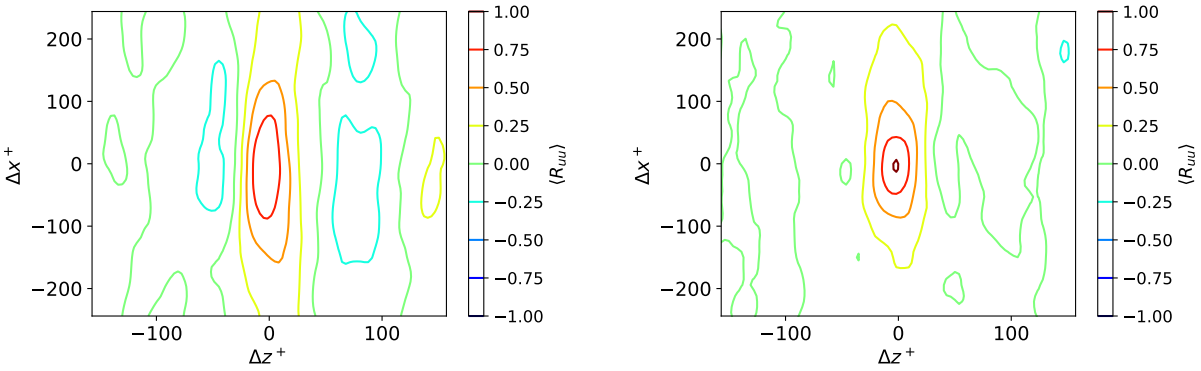

(a) Uncontrolled flow

(b) Plasma-actuated flow

Figure 8: Mean normalized two-point autocorrelations of streamwise velocity fluctuations $\langle R_{uu} \rangle$ for (a) the un-controlled and (b) the plasma-actuated flows, evaluated at $y^+ = 10$.

5 Conclusions and outlook

In this study we presented a numerical framework to investigate optimal flow control parameters to control a channel flow with arrays of plasma actuators lain to mimic the oscillating wall forcing. These were included in a DNS solver by means of their induced body force field computed with a physical model of the actuators.

Laminar flow simulations were carried out within the optimization process. These showed that the PAs managed to recreate a spanwise velocity profile at the center plane comparable to that of a drag reducing oscillating wall, with a set of parameters that are reproducible by a PA array [11]. However, when the same optimal control parameters were evaluated for the case of a turbulent flow, at the same bulk flow, no overall drag reduction was reported. Nevertheless, the observed behavior in the proximity

of the wall suggests that the actuation might weaken the streamwise coherence of turbulence structures and that it has a strong effect on the streamwise velocity variance.

Overall, this study highlights the challenges of using arrays of plasma actuators to induce a flow forcing similar to the one induced by oscillating the wall. While they appear to be effective in disrupting the turbulence coherence, which usually leads to positive drag reducing effects, they also induce strong wall-normal motions which instead drag high momentum fluid towards the wall, thus increasing the local (in space and time) friction. We presented a way to optimize the geometrical and operational PAs parameters towards finding the best flow control configuration. While the chosen approach – optimization on laminar flows aimed at replicating a drag-reducing Stokes flow – showed its limitations, the developed framework can be directly deployed on turbulent flows.

Acknowledgments
This study was carried out within the "WAll-Turbulence Active COntrol" project - funded by the European Union - Next Generation EU within the PRIN 2022 PNRR program (D.D.1409 of the 14/09/2022 Ministero dell'Università e della Ricerca). E. Fracchia was also supported by the GREENER project — funded by the European Union — Next Generation EU within the PRIN 2022 program (D.D. 104 - 02/02/2022 Ministero dell'Universitá e della Ricerca). This manuscript reflects only the authors' views and opinions and the Ministry cannot be considered responsible for them.

References

[1] R. García-Mayoral and J. Jiménez. Drag reduction by riblets. *Philosophical transactions of the Royal society A: Mathematical, physical and engineering Sciences*, 369(1940):1412–1427, 2011.

[2] Kwing-So Choi. Near-wall structure of a turbulent boundary layer with riblets. *Journal of fluid mechanics*, 208:417–458, 1989.

[3] G. Cafiero and G. Iuso. Drag reduction in a turbulent boundary layer with sinusoidal riblets. *Experimental Thermal and Fluid Science*, 139:110723, 2022.

[4] G. Cafiero, E. Amico, and G. Iuso. Manipulation of a turbulent boundary layer using sinusoidal riblets. *Journal of Fluid Mechanics*, 984:A59, 2024.

[5] L. Agostini, E. Touber, and M. A. Leschziner. The turbulence vorticity as a window to the physics of friction-drag reduction by oscillatory wall motion. *International Journal of Heat and Fluid Flow*, 51:3–15, 2015.

[6] K.-S. Choi and M. Graham. Drag reduction of turbulent pipe flows by circular-wall oscillation. *Physics of Fluids*, 10(1):7–9, 1998.

[7] M. Quadrio and S. Sibilla. Numerical simulation of turbulent flow in a pipe oscillating around its axis. *Journal of Fluid Mechanics*, 424:217–241, 2000.

[8] P. Ricco, M. Skote, and M. A. Leschziner. A review of turbulent skin-friction drag reduction by near-wall transverse forcing. *Progress in Aerospace Sciences*, 123:100713, 2021.

[9] T. Jukes, K.-S. Choi, G. Johnson, and S. Scott. Turbulent drag reduction by surface plasma through spanwise flow oscillation. In *3rd AIAA Flow Control Conference*, page 3693, 2006.

[10] O. Mahfoze and S. Laizet. Skin-friction drag reduction in a channel flow with streamwise-aligned plasma actuators. *International Journal of Heat and Fluid Flow*, 66:83–94, 2017.

[11] M. T. Hehner, D. Gatti, and J. Kriegseis. Stokes-layer formation under absence of moving parts—a novel oscillatory plasma actuator design for turbulent drag reduction. *Physics of Fluids*, 31(5), 2019.

[12] G. Neretti, P. Seri, M. Taglioli, A. Shaw, F. Iza, and C. A. Borghi. Geometry optimization of linear and annular plasma synthetic jet actuators. *Journal of Physics D: Applied Physics*, 50(1):015210, 2016.

[13] N. Benard, J.-P. Bonnet, and E. Moreau. Drag reduction by wall-parallel standing wave with plasma actuator. In *AIAA SCITECH 2024 Forum*, page 1512, 2024.

[14] N. Benard and E. Moreau. Electrical and mechanical characteristics of surface ac dielectric barrier discharge plasma actuators applied to airflow control. *Experiments in Fluids*, 55(11):1846, 2014.

[15] S. Zhi, Z. Haohua, L. Jun, X. Like, L. Xuecheng, K. Weiliang, and Others. Minimizing airfoil drag at low angles of attack with dbd-based turbulent drag reduction methods. *Chinese Journal of Aeronautics*, 36(4):104–119, 2023.

[16] H. Zong, Z. Su, H. Liang, and Y. Wu. Experimental investigation and reduced-order modeling of plasma jets in a turbulent boundary layer for skin-friction drag reduction. *Physics of Fluids*, 34(8), 2022.

[17] D. Elam. *A direct numerical simulation of dielectric barrier discharge (DBD) plasma actuators for turbulent skin-friction control*. PhD thesis, University of Warwick, 2012.

[18] A. Malli. Dns study of turbulent drag reduction via dbd plasma actuators. 2019.

[19] M. Quadrio and P. Luchini. The numerical solution of the incompressible navier–stokes equations on a low-cost, dedicated parallel computer. *Preprint*, 2004.

[20] P. Luchini and M. Quadrio. A low-cost parallel implementation of direct numerical simulation of wall turbulence. *Journal of Computational Physics*, 211(2):551–571, 2006.

[21] J. Jiménez and P. Moin. The minimal flow unit in near-wall turbulence. *Journal of Fluid Mechanics*, 225:213–240, 1991.

[22] Y. Suzen, G. Huang, J. Jacob, and D. Ashpis. Numerical simulations of plasma based flow control applications. In *35th AIAA Fluid Dynamics Conference and Exhibit*, page 4633, 2005.

[23] R. A. Bernal-Orozco, I. Carvajal-Mariscal, and O. M. Huerta-Chavez. Flow and performance effects of a phenomenological model for a dbd actuator under different operating parameters. *Journal of the Brazilian Society of Mechanical Sciences and Engineering*, 45(10):513, 2023.

[24] J. Yao, X. Chen, F. Thomas, and F. Hussain. Large-scale control strategy for drag reduction in turbulent channel flows. *Physical Review Fluids*, 2(6):062601, 2017.

[25] The MathWorks Inc. statistics and machine learning toolbox documentation, 2022.

[26] X.Q. Cheng, C.W. Wong, F. Hussain, W. Schröder, and Y. Zhou. Flat plate drag reduction using plasma-generated streamwise vortices. *Journal of Fluid Mechanics*, 918:A24, 2021.

[27] M. Quadrio and P. Ricco. Critical assessment of turbulent drag reduction through spanwise wall oscillations. *Journal of Fluid Mechanics*, 521:251–271, 2004.

[28] R. D. Moser, J. Kim, N. N. Mansour, and Others. Direct numerical simulation of turbulent channel flow up to re= 590. *Physics of Fluids*, 11(4):943–945, 1999.